Cellular/Molecular

Preferential Localization of Muscarinic M_1 Receptor on Dendritic Shaft and Spine of Cortical Pyramidal Cells and Its Anatomical Evidence for Volume Transmission

Miwako Yamasaki,[1] Minoru Matsui,[2] and Masahiko Watanabe[1,3]

[1]Department of Anatomy, Hokkaido University Graduate School of Medicine, Sapporo 060-8638, Japan, [2]Department of Clinical Research and General Medicine, Tokyo-Nishi Tokushukai Hospital, Tokyo, 196-0003, Japan, and [3]Japan Science and Technology Agency, Core Research for Evolutional Science and Technology (CREST), Sanbocho, Chiyada-ku, Tokyo 102-0075, Japan

Acetylcholine (ACh) plays important roles for higher brain functions, including arousal, attention, and cognition. These effects are mediated largely by muscarinic acetylcholine receptors (mAChRs). However, it remains inconclusive whether the mode of ACh-mAChR signaling is synaptic, so-called "wired," transmission mediated by ACh released into the synaptic cleft, or nonsynaptic, so-called "volume," transmission by ambient ACh. To address this issue, we examined cellular and subcellular distribution of M_1, the most predominant mAChR subtype in the cerebral cortex and hippocampus, and pursued its anatomical relationship with cholinergic varicosities in these regions of adult mice. M_1 was highly expressed in glutamatergic pyramidal neurons, whereas it was low or undetectable in various GABAergic interneuron subtypes. M_1 was preferentially distributed on the extrasynaptic membrane of pyramidal cell dendrites and spines. Cholinergic varicosities often made direct contact to pyramidal cell dendrites and synapses. At such contact sites, however, synapse-like specialization was infrequent, and no particular accumulation was found at around contact sites for both M_1 and presynpatic active zone protein Bassoon. These features contrasted with those of the glutamatergic system, in which AMPA receptor GluA2 and metabotropic receptor mGluR5 were recruited to the synaptic or perisynaptic membrane, respectively, and Bassoon was highly accumulated in the presynaptic terminals. These results suggest that M_1 is so positioned to sense ambient ACh released from cholinergic varicosities at variable distances, and to enhance the synaptic efficacy and excitability of pyramidal cells. These molecular–anatomical arrangements will provide the evidence for volume transmission, at least in M_1-mediated cortical cholinergic signaling.

Introduction

The cerebral cortex and hippocampus receive prominent cholinergic inputs from the basal forebrain (Mesulam et al., 1983), and acetylcholine (ACh) plays important roles for arousal, attention, and cognitive processes (Hasselmo, 2006; Briand et al., 2007). These functions are mediated largely by muscarinic acetylcholine receptors (mAChRs) (Bartus et al., 1982; Iversen et al., 1997). Five subtypes of mAChRs have been identified and classified into two subfamilies: the M_1-like subfamily (M_1, M_3, and M_5) is coupled to $G\alpha_{q/11}$ protein, leading to activation of phospholipase C, whereas the M_2-like subfamily (M_2 and M_4) is coupled to $G_{i/o}$, which inhibits adenylate cyclase (Matsui et al., 2004). In general, mAChR activation modulates multiple ionic conductances and depolarizes cortical pyramidal cells, thereby enhancing the generation and backpropagation of action potential (Krnjevic et al., 1971; McCormick and Prince, 1985; Tsubokawa and Ross, 1997; Gulledge and Stuart, 2005; Gulledge et al., 2009; Yan et al., 2009). Furthermore, mAChR activation induces network oscillations (Fisahn et al., 1998, 2002; Traub et al., 2004), and modulates the induction and amplitude of long-term potentiation (LTP) at hippocampal synapses (Huerta and Lisman, 1993; Shinoe et al., 2005).

However, it remains inconclusive whether the major mode of cholinergic signaling is synaptic, so-called "wired," transmission mediated by ACh released into the synaptic cleft, or nonsynaptic, so-called "volume," transmission by ambient ACh (Zoli and Agnati, 1996; Descarries et al., 1997; Vizi, 2000; Sarter et al., 2009). Volume transmission is inferred from observations that cholinergic fibers are diffuse and rough in topographical organization (Zaborszky et al., 1999), are distributed at much lower densities than ACh receptor binding sites (reviewed by Herkenham, 1987), and make synaptic specialization only infrequently (Chedotal et al., 1994; Umbriaco et al., 1994, 1995; Vaucher and Hamel, 1995; Mechawar et al., 2000, 2002; for review, see Descarries and Mechawar, 2000). On the other hand, the possibility that the signaling mode is more specific than volume transmission is also suggested from phasic ACh rise in the prefrontal cortex of task-performing rats (Parikh et al., 2007), transient mAChR-mediated modulation of cortical pyramidal cells (Gulledge and Stuart, 2005; Gulledge et al., 2009), and formation of "conventional" synapses

Received Nov. 18, 2009; revised Jan. 20, 2010; accepted Feb. 7, 2010.

This study was supported through Special Coordination Funds for Promoting Science and Technology, Grants-in-Aid for Scientific Research (S) (19100005 to M.W.), and Grants-in-Aid for Scientific Research on Priority Area (17023001 to M.W.) provided by the Ministry of Education, Culture, Sports, Science and Technology of Japan.

Correspondence should be addressed to Masahiko Watanabe, Department of Anatomy, Hokkaido University Graduate School of Medicine, Sapporo 060-8638, Japan. E-mail: watamasa@med.hokudai.ac.jp.

DOI:10.1523/JNEUROSCI.5719-09.2010

Copyright © 2010 the authors 0270-6474/10/304408-11$15.00/0

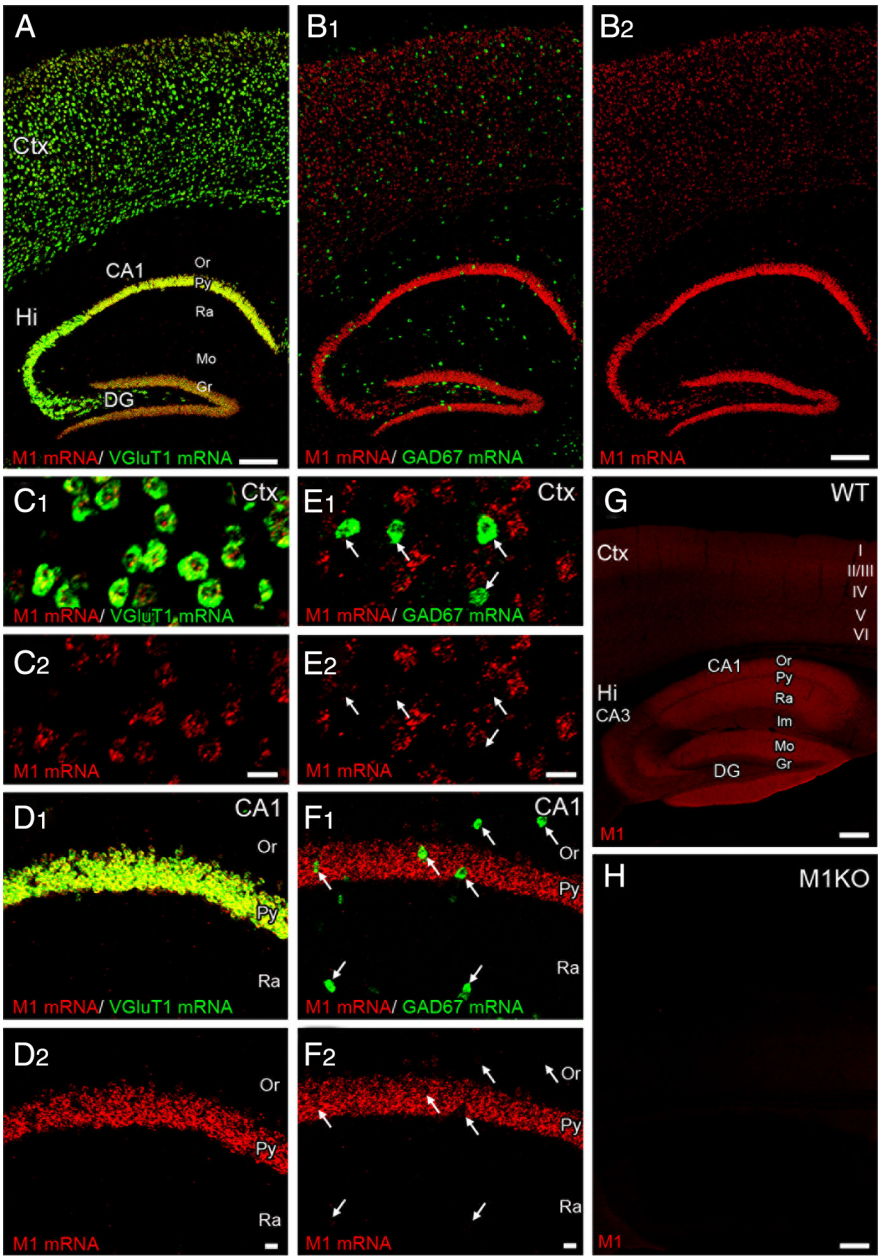

Figure 1. M_1 mRNA is preferentially expressed in cortical pyramidal cells. ***A***, ***C***, ***D***, Double-fluorescent *in situ* hybridization for M_1 (red) and VGluT1 (green) in the cortex (***A***, ***C***) and hippocampus (***A***, ***D***). Signals for M_1 and VGluT1 mRNAs extensively overlap with each other. ***B***, ***E***, ***F***, Double-fluorescent *in situ* hybridization for M_1 (red) and GAD67 (green) in the cortex (***B***, ***E***) and hippocampus (***B***, ***F***). M_1 mRNA is faint or negative in GAD67 mRNA-expressing cells (***E***, ***F***, arrows). ***G***, ***H***, Immunofluorescence for M_1 protein in wild-type (***G***) and M_1 knock-out (***H***) brains. Ctx, Cerebral cortex; I–VI, layer I–VI of the cerebral cortex; Hi, hippocampus; CA1 and CA3, CA1 and CA3 region of the Ammon's horn; DG, dentate gyrus; Or, stratum oriens; Py, pyramidal cell layer; Ra, stratum radiatum; lm, stratum lacunosum-moleculare; Mo, molecular layer; Gr, granule cell layer. Scale bars, 200 μm (***A***, ***B***, ***G***, and ***H***); 10 μm (***C–F***).

by cholinergic fibers (Frotscher and Leranth, 1985; Smiley et al., 1997; Turrini et al., 2001).

To answer this question, we examined the molecular–anatomical relationship between cholinergic varicosities and M_1, the most predominant subtype in the cerebral cortex and hippocampus (Levey et al., 1991, 1995). M_1 was preferentially expressed in pyramidal cells and enriched on the extrasynaptic membrane of their dendrites and spines. Pyramidal cell dendrites and spines were often contacted by cholinergic fibers and varicosities. However, M_1 clusters far more outnumbered cholinergic varicosities, and showed no particular accumulation toward cholinergic varicosities or at their contact sites. Moreover, synapse-like specializations were infrequently observed at such contact sites. These results suggest that M_1 is so placed to modulate the synaptic efficacy and excitability of pyramidal cells by sensing ambient ACh, and thus support the concept of volume transmission, at least, for M_1-mediated cholinergic transmission in the cortex and hippocampus.

Materials and Methods

Animal and section preparation. All experiments were performed according to the guidelines laid down by the animal welfare committees of Hokkaido University. Adult C57BL/6 mice and M_1 knock-out mice were used. The generation and characterization of M_1 knock-out mice have been described previously (Ohno-Shosaku et al., 2003). Under deep pentobarbital anesthesia (100 mg/kg of body weight, i.p.), mice were fixed transcardially with 4% paraformaldehyde in 0.1 M sodium phosphate buffer (PB, pH 7.2) for light microscopy or 4% paraformaldehyde/0.1% glutaraldehyde in PB for electron microscopy. Sections of fixed brains (50 μm in thickness) were prepared by microslicer (VT1000S, Leica Microsystems) and subjected to free-floating immunohistochemistry. Ultrathin cryosections (150 nm) were also prepared by ultracryomicrotome (EM-FCS; Leica Microsystems). For *in situ* hybridization, brains were freshly obtained under deep pentobarbital anesthesia and immediately frozen in powdered dry ice. Fresh frozen sections (20 μm) were cut on a cryostat (CM1900; Leica Microsystems). All sections were mounted on silane-coated glass slides.

In situ *hybridization.* Digoxigenin (DIG)- or fluorescein-labeled cRNA probes were prepared to detect multiple mRNAs simultaneously. Complementary DNA fragments of mouse mAChR M_1 cDNA (nucleotides 1217-2009; GenBank accession number, NM_001112697), mouse mAChR M_3 cDNA (1662-2524; NM_033269), mouse 67 kDa-glutamic acid decarboxylase (GAD67) cDNA (1036-2015; NM_008077), mouse type 1 vesicular glutamate transporter (VGluT1) cDNA (301-1680; BC054462), and rat somatostatin cDNA (133-408, NM_012659) were subcloned into the Bluescript II plasmid vector. Preparation of cRNA probes was performed as previously described (Yamasaki et al., 2001). Overall hybridization pattern in the brain with use of each probe is shown in supplemental Figure S1, available at www.jneurosci.org as supplemental material.

Sections were treated with the following incubation steps: fixation with 4% paraformaldehyde–PB, pH 7.2, for 10 min; washing in PBS, pH 7.2, for 10 min; acetylation with 0.25% acetic anhydride in 0.1 M triethanolamine-HCl, pH 8.0, for 10 min; and prehybridization for 1 h in a hybridization buffer (50% formamide, 50 mM Tris-HCl, pH 7.5, 0.02% Ficoll, 0.02% polyvinylpyrrolidone, 0.02% bovine serum albumin, 0.6 M NaCl, 200 μg/ml of tRNA, 1 mM EDTA, and 10% dextran sulfate). Hybridization was performed at 63.5°C for 12 h in the hybridization buffer

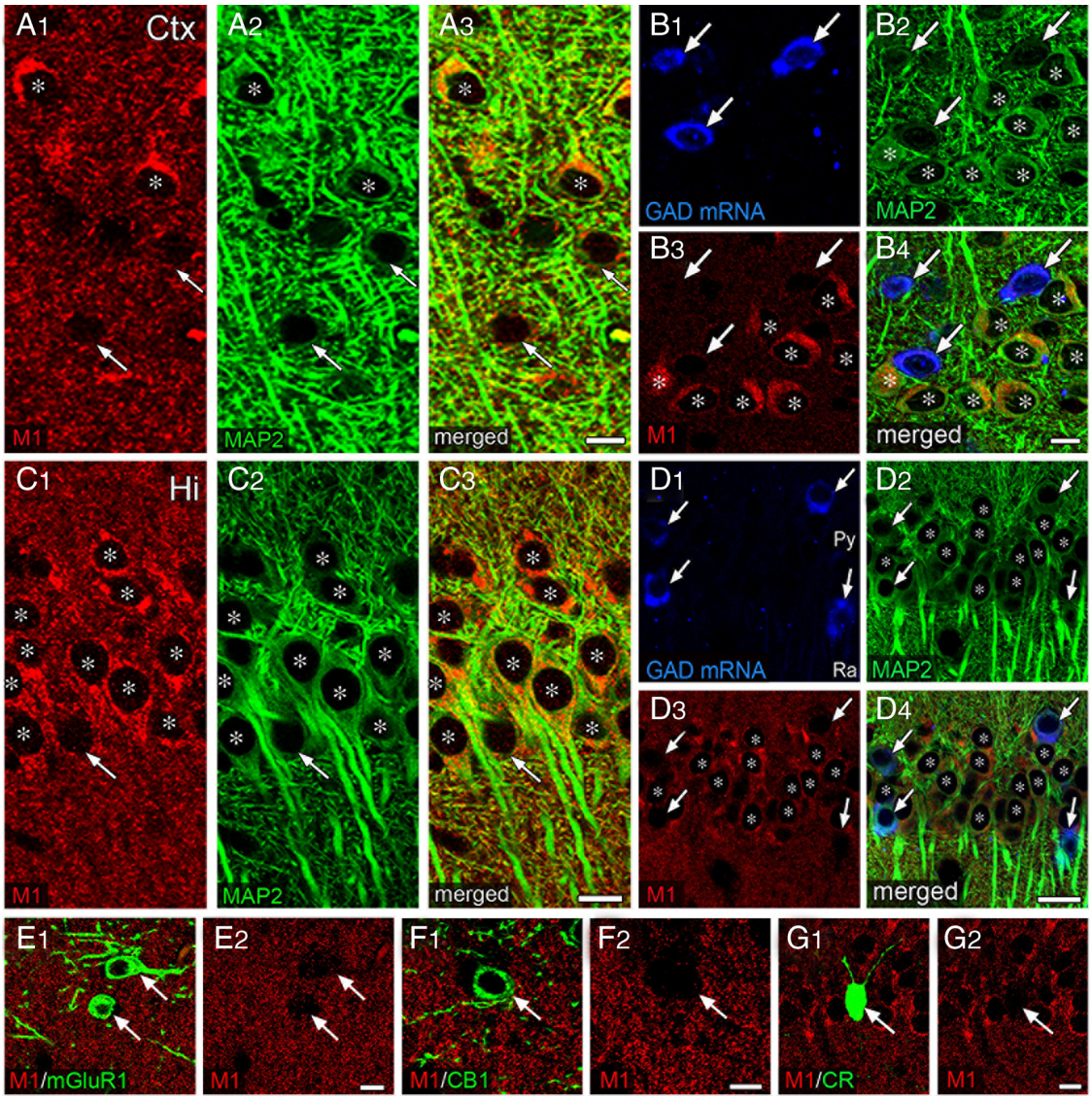

Figure 2. M_1 is preferentially distributed in pyramidal cell perikarya and neuropils of the cerebral cortex and hippocampus. ***A***, ***C***, Double immunofluorescence for M_1 (red) and MAP2 (green) in layer II/III of the cerebral cortex (***A***) and hippocampal CA1 (***C***). In addition to punctuate labeling in neuropils, intense M_1 labeling was observed in pyramidal cell perikarya labeled strongly for MAP2 (asterisk). Note low or negative M_1 labeling in perikarya weakly labeled for MAP2 (arrows in ***A*** and ***C***). ***B***, ***D***, Immunofluorescence for M_1 (red) and MAP2 (green) combined with fluorescent *in situ* hybridization for GAD67 mRNA (blue) in the cerebral cortex (***B***) and hippocampal CA1 (***D***). Compared with GAD67 mRNA-negative perikarya (asterisks), GAD67 mRNA-positive perikarya (arrows) are low or negative for M_1. ***E–G***, Double immunofluorescence for M_1 (red) and interneuron markers (green), including mGluR1a (***E***), cannabinoid receptor CB1 (***F***), and calretinin (CR, ***G***). Scale bars, 10 μm.

supplemented with cRNA probes at a dilution of 1:1000. Posthybridization washing was done at 61°C successively with 5× SSC for 30 min, 4× SSC containing 50% formamide for 40 min, 2× SSC containing 50% formamide for 40 min, and 0.1× SSC for 30 min. Sections were dipped at room temperature in NTE buffer (0.5 M NaCl, 0.01 M Tris-HCl [pH7.5], and 5 mM EDTA) for 20 min, 20 mM iodoacetamide in NTE buffer for 20 min, and TNT buffer (0.1 M Tris-HCl [pH 7.5] and 0.15 M NaCl) for 20 min.

For immunohistochemical detection, sections were blocked with 0.6% H_2O_2 in TNT buffer for 10 min, DIG blocking solution (1% blocking reagent [Roche Diagnostics], 10% normal sheep serum in TNT buffer) for 30 min, and 0.5% TSA blocking reagent (PerkinElmer) in TNT buffer for 30 min. Sections were first subjected to detection of fluorescein-labeled cRNA probe (M_1 or M_3) using peroxidase-conjugated anti-fluorescein antibody in DIG blocking solution (Roche Diagnostics, 1:500) for 1 h and the FITC-TSA plus amplification kit (PerkinElmer). After inactivation of residual peroxidase activity by 0.6% H_2O_2 in TNT buffer for 30 min, sections were subjected to the second detection of DIG-labeled cRNA probe (GAD67, VGluT1, or somatostatin) using peroxidase-conjugated anti-DIG antibody (Roche Diagnostics, 1:500) and the Cy3-TSA plus amplification kit (PerkinElmer). All of the washing and incubation solutions contained 0.0005% Tween 20.

For *in situ* hybridization combined with immunofluorescence, microslicer sections were first processed for the former incubation and detection and then subjected to the latter.

Antibodies. We used the following primary antibodies; mouse anti-Bassoon (Assay Designs), guinea pig anti-cannabinoid receptor CB1 (Fukudome et al., 2004), rabbit anti-mouse M_1 (Narushima et al., 2007), goat or guinea-pig anti-high affinity choline transporter-1 (CHT1; Miura et al., 2006), rabbit anti-calretinin (Swant), rabbit anti-GluA2 subunit of AMPA receptors (Fukaya et al., 2006), guinea-pig anti-pan-AMPA receptor (Fukaya et al., 2006), rabbit anti-GluN1 subunit of NMDA receptors (NR1; Abe et al., 2004), goat anti-microtubule-associated protein-2 (MAP2; Miura et al., 2006), guinea pig anti-metabotropic glutamate receptor mGluR1α (Uchigashima et al., 2007), rabbit anti-mGluR5 (Uchigashima et al., 2007), sheep anti-neuropeptide Y (NPY; Millipore Bioscience Research Reagents), guinea pig anti-neuronal nitric oxide synthase (Narushima et al., 2007), goat anti-parvalbumin (Miura et al., 2006), rabbit anti-VGluT1 (Miura et al.,

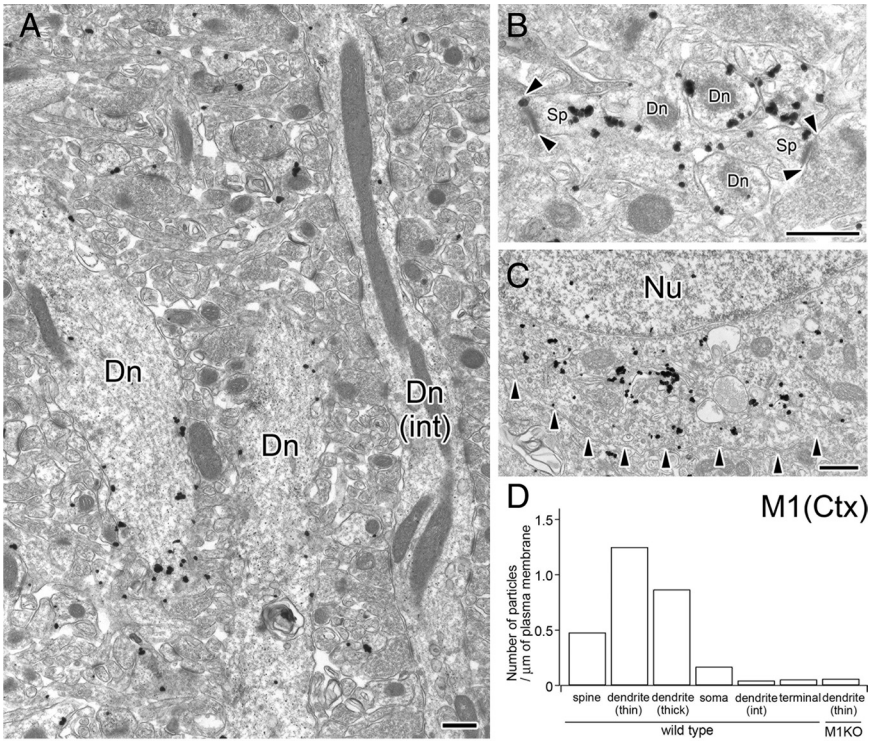

Figure 3. Preembedding immunogold electron microscopy showing abundant localization of M_1 on pyramidal cell dendrites and spines in the cortical layer II/III–IV. ***A***, Immunoparticles for M_1 are distributed on the surface of dendritic shafts of pyramidal cells (Dn). Note that M_1 labeling is almost absent from dendrites of putative inhibitory interneurons (Dn[int]). ***B***, Preferential surface expression of M_1 in small-caliber dendrites (Dn) and dendritic spines (Sp) forming asymmetrical synapses (arrowheads). ***C***, In pyramidal cell perikarya, immunoparticles for M_1 are heavily deposited around membranous organelles, but very rare on the plasma membrane (arrowheads). ***D***, The mean number of immunoparticles for M_1 per 1 μm of the plasma membrane of spines (the total measured length, 438.9 μm), thin pyramidal cell dendrites (smaller than 0.66 μm in caliber) (270.7 μm), thick pyramidal cell dendrites (larger than 0.66 μm in caliber) (204.0 μm), pyramidal cell somata (96.0 μm), interneuron dendrites (113.3 μm), presynaptic terminals (519.3 μm), and thin pyramidal cell dendrites from M_1 knock-out mice (163.44 μm). The mean diameter of sampled pyramidal cell dendrites in the cortical layer II/III was 0.66 μm. Nu, Nucleus of pyramidal cell. Scale bars: ***A–C***, 500 nm.

2006), and rabbit anti-vesicular acetylcholine transporter (VAChT; Uchigashima et al., 2007).

Immunofluorescence. All immunohistochemical incubations were done at room temperature. Microslicer sections and ultrathin cryosections were incubated successively with 10% normal donkey serum for 20 min, mixture of primary antibodies overnight (1 μg/ml), and mixture of Alexa 488-, Cy3-, or Cy5-labeled species-specific secondary antibodies for 2 h at a dilution of 1:200 (Invitrogen; Jackson ImmunoResearch). Images were taken with a confocal laser scanning microscope FV1000 (Olympus).

Immunoelectron microscopy. For preembedding immunogold electron microscopy, microslicer sections were incubated in 5% bovine serum albumin (BSA)/0.02% saponin/PBS for 30 min and then in primary antibodies diluted with 1% BSA/0.004% saponin/PBS overnight. Secondary antibodies linked to 1.4 nm gold particles (Nanogold; Nanoprobes) were then incubated for 2 h, and immunogold particles were intensified with a silver enhancement kit (HQ silver; Nanoprobes). For double immunoelectron microscopy, specimens were incubated with mixture of primary antibodies, followed by intensification with silver enhancement kit and then by immunoperoxidase reaction. Sections were further treated with 1% osmium tetroxide for 15 min, stained with 2% uranyl acetate for 30 min, dehydrated, and embedded in Epon 812.

For postembedding immunogold, slices were cryoprotected with 30% glycerol in PB, and frozen rapidly with liquid propane in the EM CPC unit (Leica Microsystems). Frozen sections were immersed in 0.5% uranyl acetate in methanol at −90°C in the AFS freeze-substitution unit (Leica Microsystems), infiltrated at −45°C with Lowicryl HM-20 resin (Chemische Werke Lowi), and polymerized with UV light. After etching with saturated sodium ethanolate solution for 1–5 s, ultrathin sections on nickel grids were treated successively with blocking solution containing 2% normal goat serum (Nichirei) in incubation solution (0.03% Triton X-100 in Tris-buffered saline, pH 7.4) for 20 min, primary antibodies (20 μg/ml for each) in incubation solution overnight, and colloidal gold (10 nm)-conjugated anti-rabbit, anti-guinea-pig, or anti-mouse IgG (1:100, British BioCell International) in blocking solution for 2 h. Finally, grids were fixed with 2% glutaraldehyde in PB for 15 min and 1% OsO_4 for 20 min and the stained with 2% uranyl acetate for 10 min and Reynold's lead citrate solution for 1 min. Photographs were taken with an H-7100 electron microscope (Hitachi).

For quantitative analysis, plasma membrane-attached immunogold particles, being defined as those apart <35 nm from the cell membrane, were counted on electron micrographs and analyzed using MetaMorph software (Molecular Devices). The mean number of membrane-attached gold particles per 1 μm of the plasma membrane was counted for each neuronal compartment (dendritic spine, dendritic shaft, soma, and presynaptic terminal). Measurements were made from two animals and pooled together, because there was no significant difference in the labeling density between the two animals. In each neuronal compartment, labeling density was calculated on individual profiles, and compared with background immunogold labeling, which was defined as labeling density of pyramidal cell dendrites in M_1 knock-out mice (smaller than 1 μm in diameter, $n = 22$ dendrites). Statistical significance of labeling density was evaluated by Mann–Whitney U test. Statistical significance of cumulative frequency was assessed by Kolmogorov–Smirnov test.

Results

M_1 is preferentially expressed in pyramidal cells

We first examined cellular expression of M_1 mRNA by fluorescent *in situ* hybridization (Fig. 1). Consistent with previous *in situ* hybridization studies using radiolabeled probes (Buckley et al., 1988; Narushima et al., 2007), antisense riboprobe reveled that M_1 mRNA was preferentially expressed in the telencephalon (supplemental Fig. S1*A*,*B*, available at www.jneurosci.org as supplemental material). M_1 mRNA-expressing cells were densely distributed in the cortex and hippocampus with the highest level in the pyramidal cell and granule cell layers of the hippocampus (Fig. 1*A–F*, red). Hybridization signals for M_1 mRNA showed distribution patterns similar to those for VGluT1 mRNA (Fig. 1*A*, green), but distinct from those for GAD67 mRNA (Fig. 1*B*, green). At a high magnification, M_1 mRNA was coexpressed in almost all neurons expressing VGluT1 mRNA ($n = 1130$ neurons in the cerebral cortex; $n = 400$ in hippocampal CA1 region) (Fig. 1*C*,*D*), whereas it was low or below the detection threshold in neurons expressing GAD67 mRNA ($n = 314$ in the cerebral cortex; $n = 117$ in hippocampal CA1 region) (Fig. 1*E*,*F*). When using the sense probes, no significant signals were yielded (data not shown). These results indicate that M_1 mRNA is preferentially ex-

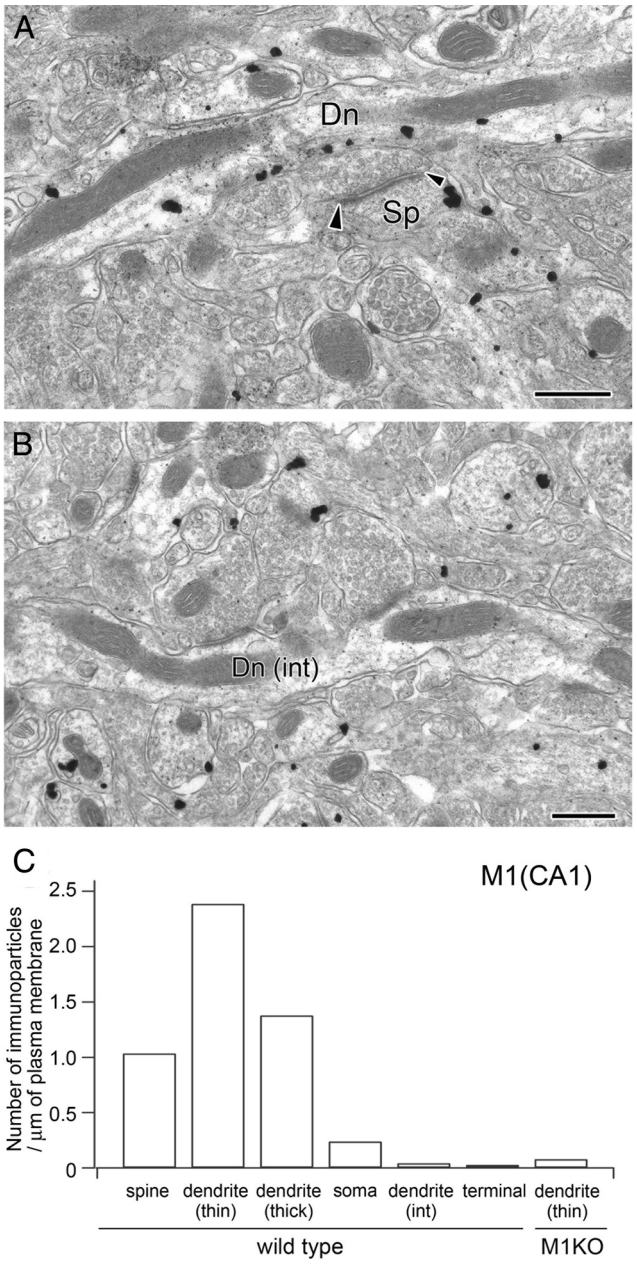

Figure 4. Preembedding immunogold electron microscopy showing abundant localization of M_1 on pyramidal cell dendrites and spines in CA1 stratum radiatum. ***A***, ***B***, Preferential M_1 localization is observed on dendritic shafts (Dn) and spines (Sp) of pyramidal cells. ***C***, The mean number of metal particles for M_1 per 1 μm of the plasma membrane of spines (the total measured length, 786.8 μm), thin pyramidal cell dendrites (smaller than 0.84 μm in caliber) (166.4 μm), thick pyramidal cell dendrites (larger than 0.84 μm in caliber) (278.5 μm), pyramidal cell somata (96.0 μm), interneuron dendrites (77.0 μm), presynaptic terminals (825.8 μm), and thin pyramidal cell dendrites from M_1 knock-out mice (84.47 μm). The mean diameter of sampled CA1 pyramidal cell dendrites was 0.84 μm. Scale bars, 500 nm.

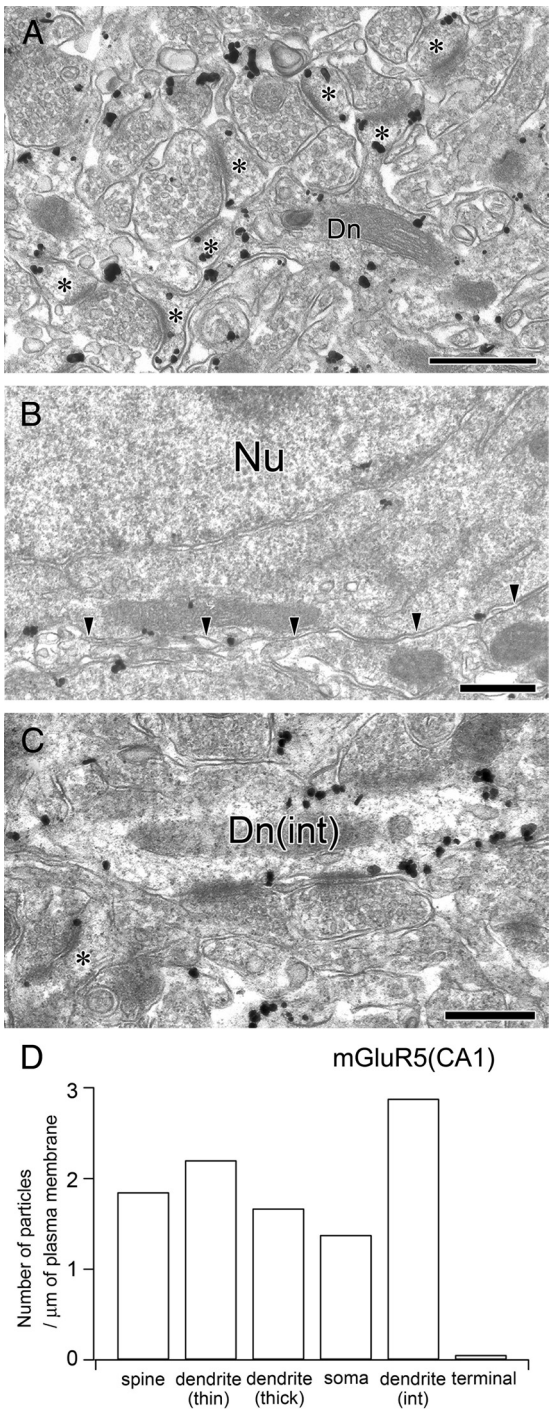

Figure 5. mGluR5 is widely distributed in somatodendritic compartments of pyramidal cells and interneurons in the hippocampal CA1. ***A–C***, Dense distribution of mGluR5 on the plasma membrane of pyramidal cell dendrites (Dn), spines (Sp), and somata (arrowheads, ***B***) as well as interneuron dendrites (Dn[int]). ***D***, The mean number of immunoparticles for M_1 per 1 μm of the plasma membrane of spines (the total measured length, 572.4 μm), thin pyramidal cell dendrites (smaller than 0.60 μm in caliber) (145.3 μm), thick pyramidal cell dendrites (larger than 0.60 μm in caliber) (129.4 μm), pyramidal cell somata (120.5 μm), interneuron dendrites (67.0 μm), and presynaptic terminals (80.6 μm). The mean diameter of sampled pyramidal cell dendrites was 0.60 μm. Nu, Nucleus of pyramidal cell. Scale bars, 500 nm.

pressed in glutamatergic or pyramidal cells in the cortex and hippocampus.

We next examined cellular and subcellular distribution of M_1 protein using specific antibody against mouse M_1 receptor (Figs. 1*G*, 2). Consistent with previous reports (Levey et al., 1991, 1995), immunofluorescence revealed that M_1 was abundant throughout the cortex and hippocampus with higher levels in layer II/III of the cerebral cortex and in the CA1 and dentate gyrus of the hippocampus (Fig. 1*G*). Control immunofluorescence in the brain of M_1 knock-out mice gave no significant staining (Fig. 1*H*), verifying the specificity of M_1 immunostaining. In both the cerebral cortex (Fig. 2*A*) and hippocampal CA1 (Fig. 2*C*), double immunofluorescence revealed that M_1 (red) was densely distrib-

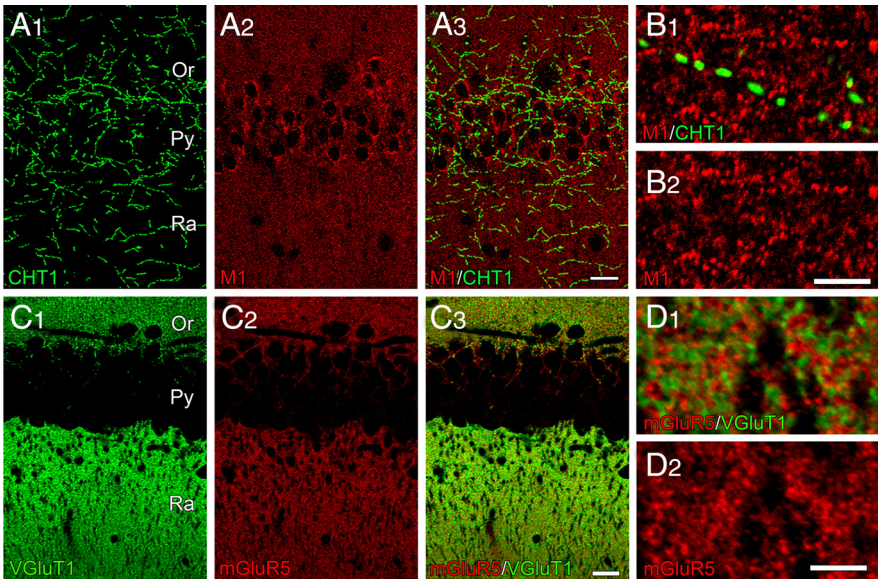

Figure 6. ***A–D***, Spatial relationship between M_1 and CHT1-labeled cholinergic varicosities (***A***, ***B***) and between mGluR5- and VGluT1-labeled glutamatergic terminals (***C***, ***D***) in CA1 stratum radiatum. ***A***, ***B***, Double immunofluorescence for CHT1 (green) and M_1 (red). Note that M_1 clusters are densely distributed with no particular accumulation around sparsely running CHT1-positive cholinergic varicosities. ***C***, ***D***, Double immunofluorescence for VGluT1 (green) and mGluR5 (red). Note that mGluR5 clusters and VGluT1-positive glutamatergic terminals show tight apposition to each other. Scale bars: ***A*** and ***C***, 10 μm; ***B*** and ***D***, 5 μm.

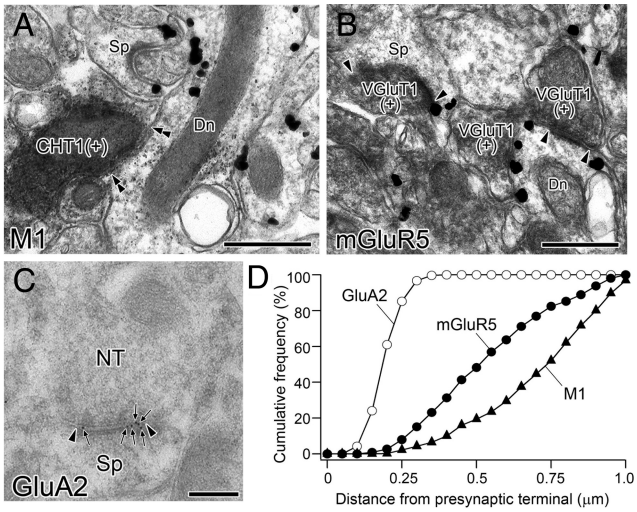

Figure 7. Immunoelectron microscopy showing loose spatial relationship between M_1 and cholinergic varicosities compared with the glutamatergic system. ***A***, Double-labeling preembedding immunoelectron microscopy for M_1 (metal particles) and CHT1 (diffuse precipitates). Accumulation of M_1 immunoparticles is not observed even at contact sites (double arrowheads). ***B***, Double-labeling preembedding immunoelectron microscopy for mGluR5 (metal particles) and VGluT1 (diffuse precipitates) showing preferential distribution on the perisynaptic membrane. Arrowheads indicate the edge of postsynaptic density. ***C***, Postembedding immunogold showing selective accumulation of GluA2 on the postsynaptic membrane (arrowheads) of asymmetrical synapse. Small arrows indicate synaptic labeling. ***D***, Cumulative frequency plots showing the distance from the center of the nearest terminals or varicosities to immunoparticles for M_1, mGluR5, and GluA2. Note differential spatial relationship between presynaptic boutons and relevant receptors. Measurements were made on postembedding immunogold for GluA2, and preembedding double-labeling immunogold for M_1-CHT1 and mGluR5-VGluT1. The number of analyzed immunoparticles: 320 particles from 54 images for GluA2; 940 from 70 images for mGluR5; 420 from 49 images for M_1. Scale bars: ***A*** and ***B***, 500 nm; ***C***, 200 nm.

uted in perikarya of MAP2 (green)-positive pyramidal cells (asterisk). In addition, M_1 was detected in the neuropil as tiny puncta on the surface of MAP2-positive dendrites. Occasionally, we encountered a few neurons, whose perikarya were faint or negative for M_1, dispersed among heavily labeled pyramidal cells (Fig. 2*A*,*C*, arrows). These neurons were likely to be GABAergic interneurons, because GAD67 mRNA-positive perikarya displayed quite low or negative immunoreactivity for M_1 (29 of 29 cells in the cerebral cortex; 16 of 16 in the hippocampal CA1 region) (Fig. 2*B*,*D*, arrows), in contrast to marked M_1 labeling in GAD67-negative ones (152 of 152 in the cerebral cortex; 355 of 355 in the hippocampal CA1 region) (Fig. 2*B*,*D*, asterisks). The scarcity of M_1 in GABAergic interneurons was further confirmed in the hippocampal CA1 by double immunofluorescence for interneuron markers, including parvalbumin (data not shown), mGluR1a (Fig. 2*E*), cannabinoid receptor CB1 (Fig. 2*F*), calretinin (Fig. 2*G*), nNOS (data not shown), and NPY (data not shown). We found that all interneurons examined were faint or below the detection threshold for M_1 in interneurons expressing parvalbumin ($n = 31$ neurons), mGluR1a ($n = 14$), CB1 ($n = 15$), calretinin ($n = 8$), nNOS ($n = 27$), and NPY ($n = 27$). These results clearly demonstrate that in both the cerebral cortex and hippocampus, M_1 mRNA and protein are preferentially expressed in glutamatergic pyramidal neurons, but quite low or negative in various subtypes of GABAergic interneurons.

M_1 is distributed on the surface of pyramidal cell dendrites and spines

Next, we investigated subcellular distribution of M_1 by immunoelectron microscopy. Since the postembedding immunogold method yielded no significant labeling in any sites of synaptic and extrasynaptic membranes (supplemental Fig. S2*A*,*B*, available at www.jneurosci.org as supplemental material), we used the preembedding silver-enhanced immunogold method.

In layer II/III of the cerebral cortex, numerous metal particles for M_1 were observed in somata, dendritic shafts, and spines of pyramidal cells, whereas they were rarely observed in somata and dendrites of putative inhibitory interneurons, as being identified from dense formation of asymmetric synapses along dendritic shafts (Fig. 3*A*). In pyramidal cell dendritic shafts and spines, the majority of metal particles were attached to the plasma membranes: the membrane-associated particles amounted to 65.3% in dendritic shaft (318 of 487 metal particles) and 90.5% (210 of 232) in dendritic spines, and the rest were found in the cytoplasm in both compartments (Fig. 3*A*,*B*). Plasma membrane-associated immunoparticles were exclusively extrasynaptic, being rarely attached to the synaptic membrane (Fig. 3*A*,*B*). In pyramidal cell somata, in contrast, a vast majority were found in the cytoplasm (90.2%, 591 of 655), in which they were associated with the Golgi apparatus and endoplasmic reticulum (Fig. 3*C*). To quantitatively compare the cell surface labeling in various subcellular compartments, we measured the density of plasma membrane-associated immunoparticles per 1 μm of the extrasynaptic plasma membrane. We used labeling density in pyramidal cell dendrites (smaller than 1 μm in diameter, $n = 22$ dendrites) of M_1 knock-out mice as the background immunogold labeling. Labeling densities in pyramidal cell dendrites and

spines were by far higher than the background ($n = 76$ dendrites; $n = 588$ spines; $p < 0.0001$ for each comparison), whereas those in inhibitory interneurons and presynaptic terminals were almost equivalent to the background level ($n = 8$ dendrites of inhibitory interneurons; $n = 588$ terminals; $p = 0.98$ and 0.21, respectively) (Fig. 3*D*). Of the labeled somatodendritic elements in pyramidal cells, M_1 was distributed in the order of thin dendrites (smaller than 0.66 μm in diameter) > thick dendrites (larger than 0.66 μm) > spines ≫ somata; 0.66 μm was the mean diameter of pyramidal cell dendrites sampled from the cortex (Fig. 3*D*).

Similar labeling patterns were observed in the pyramidal cell layer and stratum radiatum of hippocampal CA1 (Fig. 4). Strong M_1 immunoreactivity was observed on the extrasynaptic surface of dendritic shafts and spines (Fig. 4*A*) and inside pyramidal cell perikarya, whereas it was almost absent from putative inhibitory interneurons (Fig. 4*B*). Quantitative analysis further confirmed preferential distribution on the surface of pyramidal cell dendrites and spines with the highest density in thin dendrites (smaller than 0.84 μm in diameter); 0.84 μm was the mean diameter of pyramidal cell dendrites sampled from the CA1 (Fig. 4*C*). Thus, M_1 is preferentially distributed on the extrasynaptic surface of dendrites and spines in cortical pyramidal cells.

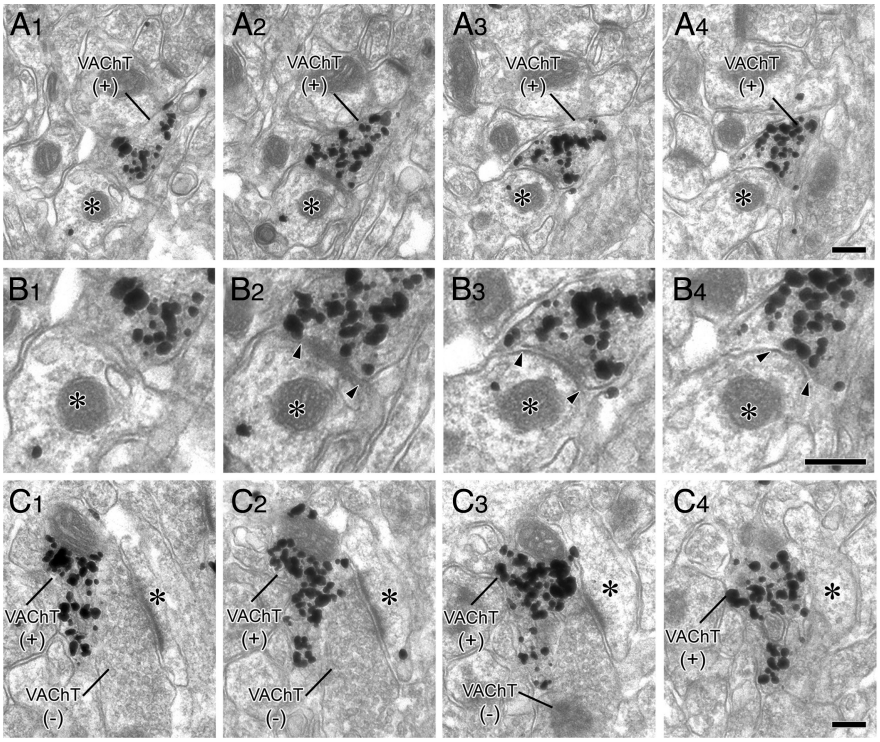

Figure 8. Cholinergic varicosities rarely make classical synapses. Consecutive images from preembedding silver-enhanced immunogold for VAChT. ***B*** shows enlarged images of ***A***. Of 30 varicosities examined, only 1 varicosity made symmetrical synapse-like contact (arrowheads) with a thin dendrite (***A***, ***B***, asterisk). Although the rest had direct contact sites with dendritic spines (***C***, asterisk) and shafts, they did not show any synaptic specializations, including parallel membrane apposition, uniform cleft width between apposed membranes, and thickening of the cytoplasmic side of apposed membranes (***C***). Scale bars, 200 nm.

Metabotropic glutamate receptor mGluR5 is another Gq-coupled receptor enriched in cortical pyramidal neurons (Lujan et al., 1996; Tanaka et al., 2000). We then examined immunohistochemical distribution of mGluR5 in the hippocampal CA1 to compare with that of M_1. Consistent with a previous study (Lujan et al., 1996), mGluR5 was abundant in somatodendritic compartments of pyramidal cells (Fig. 5*A*,*B*). Quantification of plasma membrane-associated metal particles revealed that the density of labeling was uniformly high in various somatodendritic compartments of pyramidal cells, including somata (Fig. 5*D*). Moreover, such a high surface labeling was also true in dendrites of inhibitory interneurons (Fig. 5*C*,*D*). Thus, compared with mGluR5, M_1 is unique in that it is highly concentrated on the surface of pyramidal cell dendrites and spines.

Loose spatial relationship between M_1 and cholinergic varicosities

To assess the mode of M_1-mediated cholinergic signaling, we investigated the spatial relationship between cholinergic varicosities (i.e., transmitter release site) and M_1 (receptor site) in the CA1 stratum radiatum, and compared it with that in the glutamatergic system. Double immunofluorescence for M_1 (red) and high-affinity choline transporter CHT1 (green), a marker of cholinergic varicosities, showed that punctate M_1 clusters far more outnumbered cholinergic varicosities, having variable distances to the nearest varicosities (Fig. 6*A*,*B*). In contrast, punctate mGluR5 clusters (red) were as dense as VGluT1-positive glutamatergic terminals (green) (Fig. 6*C*,*D*). Importantly, M_1 clusters were distributed with no particular accumulation or gradient toward CHT1-positive cholinergic varicosities (Fig. 6*B*), whereas mGluR5 clusters and VGluT1-positive glutamatergic terminals were apposed closely to each other (Fig. 6*D*).

Double immunoelectron microscopy confirmed and further substantiated their difference (Fig. 7). The vast majority of M_1 immunoparticles were distributed widely on the extrasyanptic membrane of pyramidal cell dendrites and spines, showing no particular accumulation toward their contact sites with CHT1-positive varicosities (Fig. 7*A*). This was also true for synapse-like contact sites having some membrane thickening or specialization on the side of pyramidal cell dendrites, although such specialized contact was encountered infrequently (32 of 1000 CHT1-positive varicosities; supplemental Fig. S3, available at www.jneurosci.org as supplemental material). In contrast, a number of mGluR5 immunoparticles were found on the perisynaptic plasma membrane of spines and dendrites that formed synaptic contacts with VGluT1-positive glutamatergic terminals (Fig. 7*B*). This was far more marked for AMPA receptor subunit GluA2, which, as detected by postembedding immunogold, was exclusively concentrated on the synaptic membrane facing putative glutamatergic terminals (Fig. 7*C*). Their different anatomical allocations between transmitter release site and receptor site were evaluated by measuring the distance from the center of the nearest terminal profiles to the center of receptor immunoparticles distributed within a 1.0-μm-radius circle from the terminals. As a function of the distance, the cumulative frequency of GluA2 particles rose most abruptly, whereas that of M_1 did most slowly (Fig. 7*D*), showing significant differences between mGluR5 and M_1 ($p < 0.05$) and between mGluR5 and GluA2 ($p < 0.0001$, Kolmogorov–Smirnov test). Therefore, M_1 far less accumulates toward transmitter release sites compared with the ionotropic and metabotropic glutamate receptors.

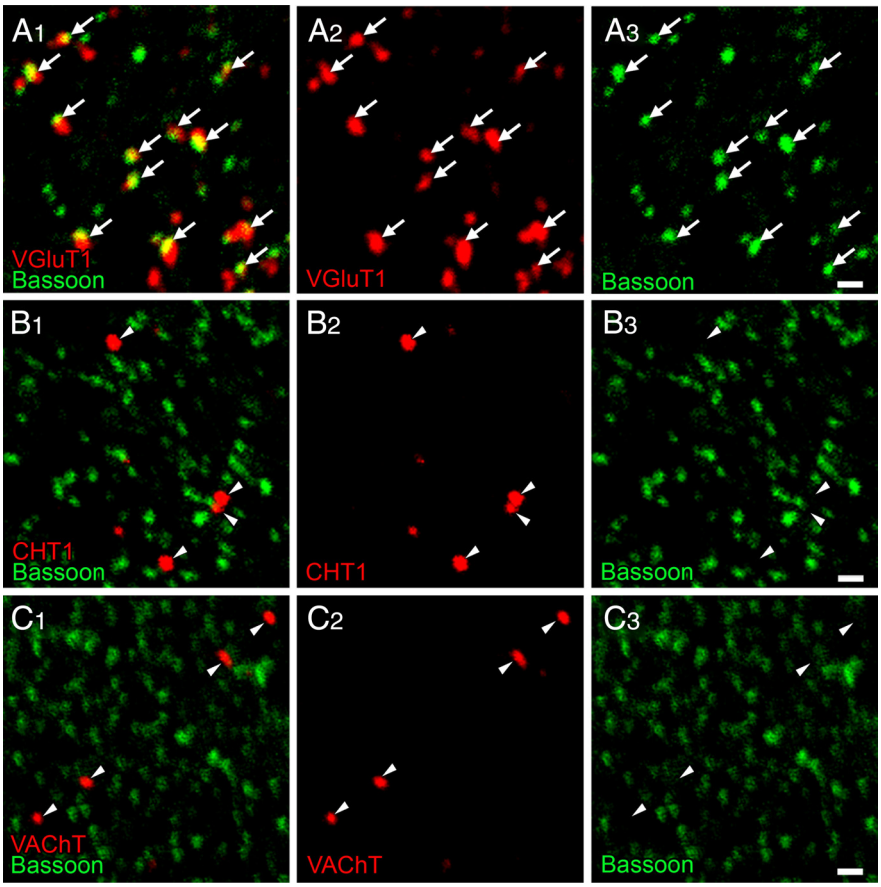

Figure 9. Bassoon is much less accumulated in cholinergic varicosities than glutamatergic terminals in the hippocampal CA1. ***A–C***, Ultrathin cryosections subjected to double immunofluorescence for active zone protein Bassoon (green) and terminal markers (red; VGluT1 in ***A***, CHT1 in ***B***, and VAChT in ***C***). The majority of VGluT1-positive glutamatergic terminals have Bassoon at one side of terminals (arrows, ***A***). In contrast, Bassoon is poorly accumulated in CHT-positive (***B***, arrowheads) or VAChT-positive cholinergic varicosities (***C***, arrowheads). Scale bar, ***A–C*** (in ***C***), 1 μm.

of 35 varicosities made synapse-like contact with a dendritic shaft (2.9%, data not shown). Therefore, these results support the notion that cholinergic varicosities rarely make classical or conventional synapses.

Finally, we asked whether and how active zone protein Bassoon accumulated in cholinergic varicosities. For this purpose, ultrathin cryosections (150 nm in thickness) were prepared to increase the spatial resolution, and subjected to double immunofluorescence for terminal or varicosity markers (Fig. 9). Many puncta labeled for Bassoon (green) were tightly apposed to VGluT1-positive glutamatergic terminals (red), and the two fluorescences overlapped at their interface (Fig. 9*A*). In contrast, Bassoon (green) was below the detection threshold in most CHT- or VAChT-positive cholinergic varicosities (red) (Fig. 9*B*,*C*). This was confirmed and further quantified by double-labeling postembedding immunoelectron microscopy. Immunogold particles for Bassoon (smaller diameter, ϕ = 10 nm) were consistently found around the active zone of VGluT1-positive terminals (larger diameter, ϕ = 15 nm) (Fig. 10*A*). Of 153 profiles of VGluT1-positive terminals forming asymmetrical synapses, 116 terminals (75.8%) had more than two immunogold particles for Bassoon (2.8 particles per varicosity) (Fig. 10*A*). In contrast, only 12.8% CHT1-positive varicosities (5 of 39; 0.49 particles per varicosity) (Fig. 10*B*), and 14.7% of VAChT-positive varicosities (5 of 34 varicosities; 0.57 particles per varicosity) (Fig. 10*C*) had more than two immunogold particles for Bassoon. Where more than two particles for Bassoon fell in cholinergic varicosities, none of synapse-like specializations were found at Bassoon-labeled sites (data not shown). Together, these results suggest that cholinergic varicosities are different from glutamatergic terminals in terms of low probability of making classical synapses both structurally and molecularly.

Cholinergic varicosities rarely make "classical" synapses

Some studies reported that the significant part of cholinergic varicosities form conventional synapses with dendritic shafts and spines (Frotscher and Leranth, 1985; Smiley et al., 1997; Turrini et al., 2001), while others described the low incidence of synaptic specializations (Aoki and Kabak, 1992; Chedotal et al., 1994; Umbriaco et al., 1994, 1995; Vaucher and Hamel, 1995; Mechawar et al., 2000, 2002). We revisited this issue by investigating the presence or absence of synapse-like specializations, including parallel membrane apposition of cholinergic varicosities and other neuronal elements, uniform cleft width between the apposed membranes, and thickening of the apposed membranes. To this end, we used serial electron microscopy for CA1 stratum radiatum, which had been subjected to preembedding immunogold microscopy for CHT1 or vesicular ACh transporter VAChT, another marker for cholinergic varicosities. Immunoparticles for VAChT were observed as dense aggregates at vesicle-accumulating varicosities of unmyelinated fibers. We prepared 10 serial sections for each of 30 VAChT-positive varicosities. Of these, only a single varicosity made synapse-like contact on to a thin dendrite (3.3%) (Fig. 8*A*,*B*). The rest of cholinergic varicosities also contacted dendrites and asymmetrical axo-spinous synapses (i.e., putative glutamatergic synapses) directly but did not show any kinds of synapse-like specializations at such contact sites (Fig. 8*C*). Similar results were obtained from CHT1-positive varicosities; only 1

Discussion

The extracellular ACh level is in the low nanomolar to micromolar range in the brain (Moor et al., 1995; Vinson and Justice, 1997). Its phasic transmission on the scale of seconds and tonic transmission on the scale of minutes modulate neuronal excitability variously (Gulledge and Stuart, 2005; Gulledge et al., 2009), and are thought to mediate precisely defined cognitive functions (Parikh et al., 2007). However, it still remains inconclusive whether cholinergic signaling in the brain takes the mode of wired or volume transmission (Zoli and Agnati, 1996; Descarries et al., 1997; Vizi, 2000; Sarter et al., 2009). To address this issue, we examined the cellular expression and subcellular localization of M_1 mAChR in the cortex and hippocampus, and further pursued its molecular–anatomical relationship with cholinergic varicosities.

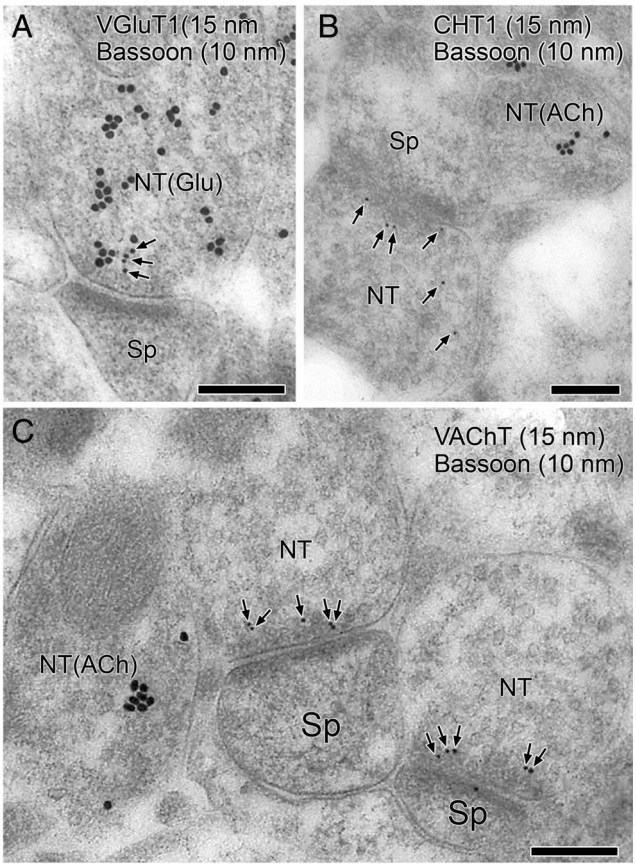

Figure 10. Cholinergic terminals are poorly equipped with Bassoon and presynaptic specialization. ***A–C***, Double-labeling postembedding immunogold for Bassoon (ϕ = 10 nm gold particles) and terminal markers (ϕ = 15 nm; VGluT1 in ***A***, CHT1 in ***B***, and VAChT in ***C***). Immunogold particles for Bassoon (small arrows) are consistently found in the cytoplasm of VGluT1-positive presynaptic terminals (NT[Glu], ***A***) or presynaptic terminals forming asymmetrical synapses onto dendritic spines (NT, ***B***, ***C***). Note that particles for Bassoon are distributed close to presynaptic membrane of asymmetrical synapses. In contrast, CHT1-positve (***B***) and VAChT-positive (***C***) cholinergic varicosities (NT[ACh]) are rarely labeled for Bassoon. Scale bars, ***A***, ***B*** (in ***B***), and ***C***, 200 nm.

M_1 is enriched on oblique dendrites of cortical pyramidal cells

The present observation that M_1 is prominently expressed in the hippocampal CA1 region and cortical layer II/III is essentially consistent with previous studies by immunohistochemistry (Levey et al., 1991, 1995) and *in situ* hybridization (Buckley et al., 1988). We have further disclosed that M_1 is preferentially expressed in glutamatergic pyramidal cells, and differentially distributed among their subcellular compartments. In both the cortex and hippocampus, a vast majority of somatic M_1 was found intracellularly and associated with the Golgi apparatus and endoplasmic reticulum, suggesting active translation and/or rich intracellular pool of M_1 in cortical pyramidal cells. Previous studies by immunoperoxidase electron microscopy showed that M_1 was abundant in postsynaptic compartments of asymmetrical synapses (Mrzljak et al., 1996; Marino et al., 1998; Rouse et al., 1998). To determine the precise subcellular localization, we conducted preembedding silver-enhanced immunogold and found that M_1 was mainly expressed on the extrasynaptic membrane of pyramidal cell dendrites and spines, rather than their synaptic membranes. The highest density of M_1 immunoparticles was observed in small-caliber dendrites (smaller than 0.84 and 0.66 μm in diameter, in the hippocampus and the cerebral cortex, respectively). In CA1 pyramidal cells, the major postsynaptic target of Schaffer collaterals is spiny dendrites <1 μm in caliber (Bannister and Larkman, 1995a,b; Megias et al., 2001). These thin dendrites are often referred to as oblique dendrites, and considered to function as single integrative compartments (Losonczy and Magee, 2006; Losonczy et al., 2008). In CA1 pyramidal cells, LTP induction leads to local changes to a given oblique dendrite, including enhancement of membrane excitability, amplitude of back-propagating action potential, and associated Ca^{2+} influx, thereby modulating future spike generation (Frick et al., 2004). Interestingly, similar effects are also induced by mAChR activation (Tsubokawa and Ross, 1997). Therefore, dense localization of M_1 on oblique dendrites could synergistically modulate the efficacy of Schaffer collateral-CA1 pyramidal cell synapses. Indeed, administration of a low concentration of carbachol (50 nM) or physiological stimulation of cholinergic fibers enhances LTP through M_1 activation (Shinoe et al., 2005). Together, M_1 enrichment in oblique dendrites will be important molecular–anatomical basis for fine-tuning of synaptic transmission and plasticity in cortical pyramidal cells.

M_1 is scarce in cortical GABAergic interneurons

Cholinergic projections from the basal forebrain target both hippocampal pyramidal cells and interneurons (Frotscher and Leranth, 1985), and augment hippocampal oscillations (reviewed by Traub et al., 2004). Furthermore, accumulating evidence that different classes of GABAergic interneurons fire preferentially at distinct time points during a given oscillation and that interneurons of a given class exhibit similar firing patterns, strongly suggests that specific interneuron subtypes have distinctive roles in shaping the activity of pyramidal cells (Klausberger and Somogyi, 2008). Thus, it is important to know which subtype of AChR is expressed in interneurons and contributes to modulation of cortical activities. The present results indicate that M_1 is expressed little, if any, in various types of cortical interneurons, including those expressing parvalbumin, CB1, mGluR1a, nNOS, NPY, or calretinin.

It has recently been shown that a specific interneuron subclass, called the O-LM cell, shows exceptionally high responsiveness to mAChR activation, including enhanced firing frequency and afterdepolarization (Lawrence et al., 2006). These effects are mediated by M_1/M_3 receptors, and associated with inhibition of an M-current and activation of a Ca^{2+}-dependent nonselective cation current (Lawrence et al., 2006). The O-LM cell places its horizontally oriented soma and dendrites in the CA1 stratum oriens, projects its axon to the lacunosum-moleculare, and expresses mGluR1a, somatostatin, and parvalbumin (Klausberger and Somogyi, 2008). However, M_1 expression in putative O-LM cells, i.e., mGluR1a-expressing interneurons, was as low as that in other interneurons, and not so prominent as that in pyramidal cells (Fig. 2*F*). To solve this discrepancy, we further pursued two possibilities that M_1 was accumulated in dendrites of O-LM cells, even if its perikaryal contents were below the detection threshold, and that M_3, instead of M_1, was abundantly expressed in O-LM cells. By confocal laser-scanning microscopy and immunoelectron microscopy, we found that M_1 expression in dendrites of putative O-LM cells, which expressed mGluR1a or bore horizontal dendrites, was around or below the detection threshold (supplemental Fig. S4, available at www.jneurosci.org as supplemental material), and that M_1 mRNA (red) was almost negative in interneurons expressing somatostatin mRNA (supplemental Fig. S5, available at www.jneurosci.org as supplemental material, green) in the CA1 stratum oriens (supplemental Fig. S5*A*, *C*, available at

www.jneurosci.org as supplemental material). Thus, the scarcity of M_1 is a general property across various types of cortical interneurons, including the O-LM cells. On the other hand, somatostatin mRNA-positive interneurons (green) expressed low but detectable levels of M_3 mRNA (red) (supplemental Fig. S5*B*,*D*, available at www.jneurosci.org as supplemental material), suggesting that the high responsiveness of O-LM cells to mAChR activation is largely mediated by M_3 rather than M_1. Recently, it has been shown in cortical pyramidal cells that transient receptor potential canonical (TRPC) is the molecular basis of mAChR-induced $G\alpha_{q/11}$/phospholipase Cβ1-mediated afterdepolarization (Yan et al., 2009). Therefore, although it remains to be tested whether this is also the case in the O-LM cells, it is also possible to assume that O-LM cells may particularly develop mechanisms that could facilitate or magnify functional linkage between mAChR and downstream effectors compared with other classes of cortical interneurons.

Volume transmission is the major mode of M_1-mediated signaling

As to the wired versus volume transmission controversy (Sarter et al., 2009), one of the central question is how transmitter release site and receptor site are spatially organized. Previous autoradiographic studies have pointed that binding sites of either nicotinic or muscarinic ACh receptors show a much denser and broader distribution pattern than cholinergic varicosities (reviewed by Herkenham, 1987). Consistent with this observation, we found that M_1 was far more densely distributed than cholinergic varicosities without showing any tendency to accumulate toward, or appose to, cholinergic varicosities. Ultrastructurally, M_1 was localized widely on the extrasynaptic membrane, being apart from cholinergic varicosities at variable distances. These anatomical features sharply contrasted to those of the glutamatergic system; GluA2 subunit and mGluR5 were accumulated to the synaptic or perisynaptic membrane, respectively, facing glutamatergic terminals. Furthermore, prominent accumulation of Bassoon, one of the cytomatrix active zone (CAZ) proteins considered to act as a platform for active zone vesicles (Richter et al., 1999), was observed near the presynaptic membrane in glutamatergic terminals, whereas no such accumulation was discernible in cholinergic varicosities. This finding implies that the molecular machinery for ACh release is not integrated into a specific site of given varicosities, unlike the active zone at glutamatergic synapses. Rather, ACh may be released to the extracellular space from various sites of varicosities. Thus, the anatomical and molecular architecture of the cholinergic system differs strikingly from that of the glutamatergic system, in that transmitter release site and receptor site are organized much more loosely in the former.

Another important clue is to understand to which extents presynaptic terminals construct synaptic contact to postsynaptic targets. Some electron microscopic studies reported that cholinergic varicosities commonly make synaptic contact in the cerebral cortex (66% in rat, Turrini et al., 2001; 67% in human, Smiley et al., 1997), while other studies reported much lower incidence [6–14% in rat hippocampus and cerebral cortex (Chedotal et al., 1994; Umbriaco et al., 1994, 1995; Vaucher and Hamel, 1995; Mechawar et al., 2000, 2002) 21% in cat visual cortex (Aoki and Kabak, 1992)]. This large difference could be attributable to differences in animal species, cortical regions, and the criteria of synaptic contact. By adopting three hallmarks of synapse-like specializations, i.e., parallel membrane apposition, uniform cleft width, and thickening of apposed membranes, our estimation in the mouse hippocampal CA1 scored extremely low rates (~3%). Beside the physical contact, one must take into consideration how relevant receptors are distributed at and around the contact sites. If we add this to our judging criteria for synaptic specializations, our low rates would be further lowered, because we observed no particular accumulation of M_1 immunoparticles at such synapse-like contact sites (supplemental Fig. S3, available at www.jneurosci.org as supplemental material). Therefore, M_1-mediated cholinergic signaling is far from typical wired transmission in many respects, and fits with the concept of volume transmission, at least, in the cortex and hippocampus.

In conclusion, M_1 is so positioned in the cortex as to sense ambient ACh released from cholinergic terminals at variable distances and to enhance the synaptic efficacy and excitability of pyramidal cells.

References

Abe M, Fukaya M, Yagi T, Mishina M, Watanabe M, Sakimura K (2004) NMDA receptor GluRε/NR2 subunits are essential for postsynaptic localization and protein stability of GluRζ1/NR1 subunit. J Neurosci 24:7292–7304.

Aoki C, Kabak S (1992) Cholinergic terminals in the cat visual cortex: ultrastructural basis for interaction with glutamate-immunoreactive neurons and other cells. Vis Neurosci 8:177–191.

Bannister NJ, Larkman AU (1995a) Dendritic morphology of CA1 pyramidal neurones from the rat hippocampus: I. Branching patterns. J Comp Neurol 360:150–160.

Bannister NJ, Larkman AU (1995b) Dendritic morphology of CA1 pyramidal neurones from the rat hippocampus: II. Spine distributions. J Comp Neurol 360:161–171.

Bartus RT, Dean RL 3rd, Beer B, Lippa AS (1982) The cholinergic hypothesis of geriatric memory dysfunction. Science 217:408–414.

Briand LA, Gritton H, Howe WM, Young DA, Sarter M (2007) Modulators in concert for cognition: modulator interactions in the prefrontal cortex. Prog Neurobiol 83:69–91.

Buckley NJ, Bonner TI, Brann MR (1988) Localization of a family of muscarinic receptor mRNAs in rat brain. J Neurosci 8:4646–4652.

Chedotal A, Umbriaco D, Descarries L, Hartman BK, Hamel E (1994) Light and electron microscopic immunocytochemical analysis of the neurovascular relationships of choline acetyltransferase and vasoactive intestinal polypeptide nerve terminals in the rat cerebral cortex. J Comp Neurol 343:57–71.

Descarries L, Mechawar N (2000) Ultrastructural evidence for diffuse transmission by monoamine and acetylcholine neurons of the central nervous system. Prog Brain Res 125:27–47.

Descarries L, Gisiger V, Steriade M (1997) Diffuse transmission by acetylcholine in the CNS. Prog Neurobiol 53:603–625.

Fisahn A, Pike FG, Buhl EH, Paulsen O (1998) Cholinergic induction of network oscillations at 40 Hz in the hippocampus in vitro. Nature 394:186–189.

Fisahn A, Yamada M, Duttaroy A, Gan JW, Deng CX, McBain CJ, Wess J (2002) Muscarinic induction of hippocampal gamma oscillations requires coupling of the M1 receptor to two mixed cation currents. Neuron 33:615–624.

Frick A, Magee J, Johnston D (2004) LTP is accompanied by an enhanced local excitability of pyramidal neuron dendrites. Nat Neurosci 7:126–135.

Frotscher M, Leranth C (1985) Cholinergic innervation of the rat hippocampus as revealed by choline acetyltransferase immunocytochemistry: a combined light and electron microscopic study. J Comp Neurol 239:237–246.

Fukaya M, Tsujita M, Yamazaki M, Kushiya E, Abe M, Akashi K, Natsume R, Kano M, Kamiya H, Watanabe M, Sakimura K (2006) Abundant distribution of TARP gamma-8 in synaptic and extrasynaptic surface of hippocampal neurons and its major role in AMPA receptor expression on spines and dendrites. Eur J Neurosci 24:2177–2190.

Fukudome Y, Ohno-Shosaku T, Matsui M, Omori Y, Fukaya M, Tsubokawa H, Taketo MM, Watanabe M, Manabe T, Kano M (2004) Two distinct classes of muscarinic action on hippocampal inhibitory synapses: M2-mediated direct suppression and M1/M3-mediated indirect suppression through endocannabinoid signalling. Eur J Neurosci 19:2682–2692.

Gulledge AT, Stuart GJ (2005) Cholinergic inhibition of neocortical pyramidal neurons. J Neurosci 25:10308–10320.

Gulledge AT, Bucci DJ, Zhang SS, Matsui M, Yeh HH (2009) M1 receptors mediate cholinergic modulation of excitability in neocortical pyramidal neurons. J Neurosci 29:9888–9902.

Hasselmo ME (2006) The role of acetylcholine in learning and memory. Curr Opin Neurobiol 16:710–715.

Herkenham M (1987) Mismatches between neurotransmitter and receptor localizations in brain: observations and implications. Neuroscience 23:1–38.

Huerta PT, Lisman JE (1993) Heightened synaptic plasticity of hippocampal CA1 neurons during a cholinergically induced rhythmic state. Nature 364:723–725.

Iversen HH, Wiklund NP, Olgart C, Gustafsson LE (1997) Nerve stimulation-induced nitric oxide release as a consequence of muscarinic M1 receptor activation. Eur J Pharmacol 331:213–219.

Klausberger T, Somogyi P (2008) Neuronal diversity and temporal dynamics: the unity of hippocampal circuit operations. Science 321:53–57.

Krnjevic K, Pumain R, Renaud L (1971) The mechanism of excitation by acetylcholine in the cerebral cortex. J Physiol 215:247–268.

Lawrence JJ, Statland JM, Grinspan ZM, McBain CJ (2006) Cell type-specific dependence of muscarinic signalling in mouse hippocampal stratum oriens interneurones. J Physiol 570:595–610.

Levey AI, Kitt CA, Simonds WF, Price DL, Brann MR (1991) Identification and localization of muscarinic acetylcholine receptor proteins in brain with subtype-specific antibodies. J Neurosci 11:3218–3226.

Levey AI, Edmunds SM, Koliatsos V, Wiley RG, Heilman CJ (1995) Expression of m1–m4 muscarinic acetylcholine receptor proteins in rat hippocampus and regulation by cholinergic innervation. J Neurosci 15:4077–4092.

Losonczy A, Magee JC (2006) Integrative properties of radial oblique dendrites in hippocampal CA1 pyramidal neurons. Neuron 50:291–307.

Losonczy A, Makara JK, Magee JC (2008) Compartmentalized dendritic plasticity and input feature storage in neurons. Nature 452:436–441.

Lujan R, Nusser Z, Roberts JD, Shigemoto R, Somogyi P (1996) Perisynaptic location of metabotropic glutamate receptors mGluR1 and mGluR5 on dendrites and dendritic spines in the rat hippocampus. Eur J Neurosci 8:1488–1500.

Marino MJ, Rouse ST, Levey AI, Potter LT, Conn PJ (1998) Activation of the genetically defined m1 muscarinic receptor potentiates *N*-methyl-D-aspartate (NMDA) receptor currents in hippocampal pyramidal cells. Proc Natl Acad Sci U S A 95:11465–11470.

Matsui M, Yamada S, Oki T, Manabe T, Taketo MM, Ehlert FJ (2004) Functional analysis of muscarinic acetylcholine receptors using knockout mice. Life Sci 75:2971–2981.

McCormick DA, Prince DA (1985) Two types of muscarinic response to acetylcholine in mammalian cortical neurons. Proc Natl Acad Sci U S A 82:6344–6348.

Mechawar N, Cozzari C, Descarries L (2000) Cholinergic innervation in adult rat cerebral cortex: a quantitative immunocytochemical description. J Comp Neurol 428:305–318.

Mechawar N, Watkins KC, Descarries L (2002) Ultrastructural features of the acetylcholine innervation in the developing parietal cortex of rat. J Comp Neurol 443:250–258.

Megias M, Emri Z, Freund TF, Gulyas AI (2001) Total number and distribution of inhibitory and excitatory synapses on hippocampal CA1 pyramidal cells. Neuroscience 102:527–540.

Mesulam MM, Mufson EJ, Wainer BH, Levey AI (1983) Central cholinergic pathways in the rat: an overview based on an alternative nomenclature (Ch1-Ch6). Neuroscience 10:1185–1201.

Miura E, Fukaya M, Sato T, Sugihara K, Asano M, Yoshioka K, Watanabe M (2006) Expression and distribution of JNK/SAPK-associated scaffold protein JSAP1 in developing and adult mouse brain. J Neurochem 97:1431–1446.

Moor E, DeBoer P, Auth F, Westerink BH (1995) Characterisation of muscarinic autoreceptors in the septo-hippocampal system of the rat: a microdialysis study. Eur J Pharmacol 294:155–161.

Mrzljak L, Levey AI, Rakic P (1996) Selective expression of m2 muscarinic receptor in the parvocellular channel of the primate visual cortex. Proc Natl Acad Sci U S A 93:7337–7340.

Narushima M, Uchigashima M, Fukaya M, Matsui M, Manabe T, Hashimoto K, Watanabe M, Kano M (2007) Tonic enhancement of endocannabinoid-mediated retrograde suppression of inhibition by cholinergic interneuron activity in the striatum. J Neurosci 27:496–506.

Ohno-Shosaku T, Matsui M, Fukudome Y, Shosaku J, Tsubokawa H, Taketo MM, Manabe T, Kano M (2003) Postsynaptic M1 and M3 receptors are responsible for the muscarinic enhancement of retrograde endocannabinoid signalling in the hippocampus. Eur J Neurosci 18:109–116.

Parikh V, Kozak R, Martinez V, Sarter M (2007) Prefrontal acetylcholine release controls cue detection on multiple timescales. Neuron 56:141– 154.

Richter K, Langnaese K, Kreutz MR, Olias G, Zhai R, Scheich H, Garner CC, Gundelfinger ED (1999) Presynaptic cytomatrix protein bassoon is localized at both excitatory and inhibitory synapses of rat brain. J Comp Neurol 408:437–448.

Rouse ST, Gilmor ML, Levey AI (1998) Differential presynaptic and postsynaptic expression of m1–m4 muscarinic acetylcholine receptors at the perforant pathway/granule cell synapse. Neuroscience 86:221–232.

Sarter M, Parikh V, Howe WM (2009) Phasic acetylcholine release and the volume transmission hypothesis: time to move on. Nat Rev Neurosci 10:383–390.

Shinoe T, Matsui M, Taketo MM, Manabe T (2005) Modulation of synaptic plasticity by physiological activation of M_1 muscarinic acetylcholine receptors in the mouse hippocampus. J Neurosci 25:11194–11200.

Smiley JF, Morrell F, Mesulam MM (1997) Cholinergic synapses in human cerebral cortex: an ultrastructural study in serial sections. Exp Neurol 144:361–368.

Tanaka J, Nakagawa S, Kushiya E, Yamasaki M, Fukaya M, Iwanaga T, Simon MI, Sakimura K, Kano M, Watanabe M (2000) Gq protein alpha subunits Galphaq and Galpha11 are localized at postsynaptic extrajunctional membrane of cerebellar Purkinje cells and hippocampal pyramidal cells. Eur J Neurosci 12:781–792.

Traub RD, Bibbig A, LeBeau FE, Buhl EH, Whittington MA (2004) Cellular mechanisms of neuronal population oscillations in the hippocampus in vitro. Annu Rev Neurosci 27:247–278.

Tsubokawa H, Ross WN (1997) Muscarinic modulation of spike backpropagation in the apical dendrites of hippocampal CA1 pyramidal neurons. J Neurosci 17:5782–5791.

Turrini P, Casu MA, Wong TP, De Koninck Y, Ribeiro-da-Silva A, Cuello AC (2001) Cholinergic nerve terminals establish classical synapses in the rat cerebral cortex: synaptic pattern and age-related atrophy. Neuroscience 105:277–285.

Uchigashima M, Narushima M, Fukaya M, Katona I, Kano M, Watanabe M (2007) Subcellular arrangement of molecules for 2-arachidonoyl-glycerol-mediated retrograde signaling and its physiological contribution to synaptic modulation in the striatum. J Neurosci 27:3663–3676.

Umbriaco D, Watkins KC, Descarries L, Cozzari C, Hartman BK (1994) Ultrastructural and morphometric features of the acetylcholine innervation in adult rat parietal cortex: an electron microscopic study in serial sections. J Comp Neurol 348:351–373.

Umbriaco D, Garcia S, Beaulieu C, Descarries L (1995) Relational features of acetylcholine, noradrenaline, serotonin and GABA axon terminals in the stratum radiatum of adult rat hippocampus (CA1). Hippocampus 5:605–620.

Vaucher E, Hamel E (1995) Cholinergic basal forebrain neurons project to cortical microvessels in the rat: electron microscopic study with anterogradely transported *Phaseolus vulgaris* leucoagglutinin and choline acetyltransferase immunocytochemistry. J Neurosci 15:7427–7441.

Vinson PN, Justice JB Jr (1997) Effect of neostigmine on concentration and extraction fraction of acetylcholine using quantitative microdialysis. J Neurosci Methods 73:61–67.

Vizi ES (2000) Role of high-affinity receptors and membrane transporters in nonsynaptic communication and drug action in the central nervous system. Pharmacol Rev 52:63–89.

Yamasaki M, Yamada K, Furuya S, Mitoma J, Hirabayashi Y, Watanabe M (2001) 3-Phosphoglycerate dehydrogenase, a key enzyme for l-serine biosynthesis, is preferentially expressed in the radial glia/astrocyte lineage and olfactory ensheathing glia in the mouse brain. J Neurosci 21:7691–7704.

Yan HD, Villalobos C, Andrade R (2009) TRPC channels mediate a muscarinic receptor-induced afterdepolarization in cerebral cortex. J Neurosci 29:10038–10046.

Zaborszky L, Pang K, Somogyi J, Nadasdy Z, Kallo I (1999) The basal forebrain corticopetal system revisited. Ann N Y Acad Sci 877:339–367.

Zoli M, Agnati LF (1996) Wiring and volume transmission in the central nervous system: the concept of closed and open synapses. Prog Neurobiol 49:363–380.